*Inorg. Chem.* **2006**, *45*, 386–394

Inorganic Chemistry Article

# Synthesis and Full Characterization of Molybdenum and Antimony Corroles and Utilization of the Latter Complexes as Very Efficient Catalysts for Highly Selective Aerobic Oxygenation Reactions

**Inna Luobeznova,† Marina Raizman,† Israel Goldberg,*,‡ and Zeev Gross*,†**

*Department of Chemistry and Institute of Catalysis Science and Technology, Technion−Israel Institute of Technology, Haifa 32000, Israel, and School of Chemistry, Tel Aviv University, Tel Aviv 69978, Israel*

Received August 30, 2005

Two molybdenum and three antimony corroles were isolated and characterized by NMR, EPR, and electrochemistry. The very negative reduction potentials of the (oxo)molybdenum(V) corroles are clearly related to their inactivity as oxygen transfer reagents and the unsuccessful attempts to isolate lower-valent molybdenum corroles. X-ray crystallography of the (oxo)molybdenum(V) corrole **1a** and the *trans*-difluoroantimony(V) corrole **2c**, the first of their kind, revealed that their molecular structures represent extreme cases of such complexes: a highly domed corrole with very large out-of-plane metal displacement for **1a** (0.73 Å) and a very flat corrole with the metal ion in its center for **2c**. All three antimony corroles displayed high activity and selectivity as catalysts for the photoinduced oxidation of thioanisole by molecular oxygen, with superior results obtained in alcoholic solvents with **2c** as catalyst. Allylic and tertiary benzylic CH bonds were also oxidized under those conditions, with absolute selectivity to the corresponding hydroperoxides.

## Introduction

Transition metal complexes of 5,10,15-tris(pentafluorophenyl)corrole[1] and similar derivatives (Chart 1) were recently

**Chart 1**

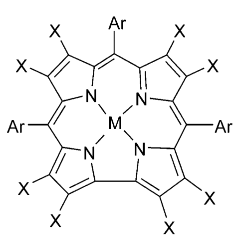


Ar = $C_6F_5$ or *o*-$C_6Cl_2H_3$
M = Cr, Fe, Mn, or Rh
X = H, F, or Br

revealed as potent catalysts for a large variety of reactions.[2] The chromium corrole-based system is particularly interesting in regard to oxidation catalysis,[3] as it relies on molecular oxygen as the oxygen atom source without requiring any additives (cooxidants, coreductants, etc.) or external forces (heat, light, pressure, etc.). In addition, both the $O_2$-activating chromium(III) and the O-transferring (oxo)chromium(V) complexes were fully characterized.[4] However, catalysis remained confined to the very oxophilic phosphines.[5] This is apparently a general limitation of first row transition metals: increased reactivity of a low-valent metal complex, $M^n$, with regard to $O_2$ activation comes at the expense of

* To whom correspondence should be addressed. E-mail: goldberg@post.tau.ac.il (I.G.); chr10zg@techunix.technion.ac.il (Z.G.).
† Technion−Israel Institute of Technology.
‡ Tel Aviv University.

(1) Gross, Z.; Galili, N.; Saltsman, I. *Angew. Chem., Int. Ed.* **1999**, *38*, 1427−1429. (b) Gross, Z.; Galili, N.; Simkhovich, L.; Saltsman, I.; Botoshansky, M.; Blaser, D.; Böse, R.; Goldberg, I. *Org. Lett.* **1999**, *1*, 599−602.

(2) Gross, Z.; Simkhovich, L.; Galili, N. *Chem. Commun.* **1999**, 599−600. (b) Gross, Z.; Golubkov, G.; Simkhovich, L. *Angew. Chem., Int. Ed.* **2000**, *39*, 4045−4047. (c) Golubkov, G.; Bendix, J.; Gray, H. B.; Mahammed, A.; Goldberg, I.; DiBilio, A. J.; Gross, Z. *Angew. Chem., Int. Ed.* **2001**, *40*, 2132−2134. (d) Simkhovich, L.; Gross, Z. *Tetrahedron Lett.* **2001**, *42*, 8089−8092. (e) Simkhovich, L.; Mahammed, A.; Goldberg, I.; Gross, Z. *Chem.*−*Eur. J.* **2001**, *7*, 1041−1045. (f) Grodkowski, J.; Neta, P.; Fujita, E.; Mahammed, A.; Simkhovich, L.; Gross, Z. *J. Phys. Chem. A* **2002**, *106*, 4772−4778. (g) Simkhovich, L.; Goldberg, I.; Gross, Z. *J. Porphyrins Phthalocyanines* **2002**, *6*, 439−444. (h) Liu, H. Y.; Lai, T. S.; Yeung, L. L.; Chang, C. K. *Org. Lett.* **2003**, *5*, 617−620. (i) Collman, J. P.; Zeng, L.; Decreau, R. A. *Chem. Commun.* **2003**, 2974−2975. (j) Wang, S. H. L.; Mandimutsira, B. S.; Todd, R.; Ramdhanie, B.; Fox, J. P.; Goldberg, D. P. *J. Am. Chem. Soc.* **2004**, *126*, 18−19. (k) Saltsman, I.; Simkhovich, L.; Balazs, Y. S.; Goldberg, I.; Gross, Z. *Inorg. Chim. Acta* **2004**, *357*, 3038−3046. (l) Mahammed, A.; Gross, Z. *J. Am. Chem. Soc.* **2005**, *127*, 2883−2887. (m) Zhang, R.; Harischandra, D. N.; Newcomb, M. *Chem.*−*Eur. J.* **2005**, *11*, 5713−5720.



10.1021/ic051483g CCC: $33.50 
Published on Web 12/13/2005

lowered reactivity of the high-valent (oxo)metal complex (O)$M^{n+2}$ for O transfer.

One way to overcome this limitation and thus extend the scope of the catalytic reactions could be the utilization of corrole complexes with heavier metal ions. In porphyrin chemistry, the $O_2$-activating ruthenium(II) and the O-transferring (dioxo)ruthenium(VI) porphyrins (note the difference of four oxidation states) were fully characterized in what remains the most proficient metal–oxo-based catalytic system for aerobic oxidation.[6] But ruthenium corroles were found not to be suitable for $O_2$ activation because of their dimerization (in the low-valent oxidation state) to very stable binuclear complexes with triply bound ruthenium.[7] Other attractive choices for oxidation catalysis are molybdenum and antimony corroles, as representatives of transition and nontransition heavy metal complexes. Molybdenum porphyrin complexes are good catalysts for epoxidation of alkenes by hydrogen peroxide because of their ability to adopt exogenous ligands that are cis rather than trans to each other,[8] and photoassisted epoxidation of alkenes has been reported with both molybdenum and antimony porphyrins.[9] Very little is known for the analogous corrole metal complexes. One (oxo)molybdenum(V) corrole was reported by Murakami et al many years ago; Gryko's group recently prepared several such complexes with triarylcorroles,[10] while Kadish and coworkers showed that antimony(III) corroles can be electrochemically oxidized to (nonisolated) antimony(IV) and antimony(V) derivatives.[11] We used corroles with electron-withdrawing substituents, required for oxidative stability, for the synthesis and isolation of the (oxo)molybdenum(V) complexes **1a** and **b** and the three antimony corroles **2a**–**c** (Chart 2). All complexes were characterized by spectroscopy and electrochemistry; **1a** and **2c** were also characterized by X-ray crystallography. Examination of the metallocorroles as oxidation catalysts revealed that the antimony complexes are very efficient catalysts for promoting photoassisted aerobic oxygenation of organic molecules in a highly selective fashion.

**Chart 2**

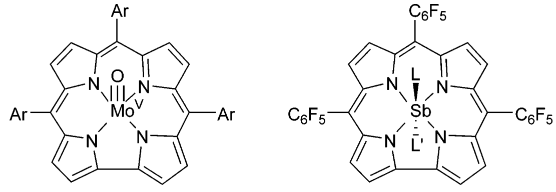

**1a**: Ar = $C_6F_5$
**1b**: Ar = *o*-$C_6Cl_2H_3$

**2a**: L = pyridine, no L'
**2b**: L = O, no L'
**2c**: L = L' = F

**Scheme 1**

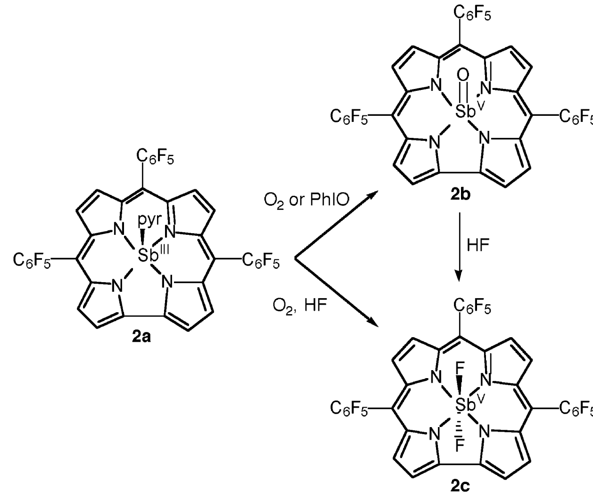


## Results and Discussion

**Synthesis.** The (oxo)molybdenum(V) complexes **1a** and **b** were obtained in 73 and 65% yields, respectively, by heating the corresponding corrole with a 5-fold excess of hexacarbonylmolybdenum for 1 h in Decaline. The easily isolated products are distinctively different from the free-base corroles: nonfluorescent, red rather than purple, NMR silent, and EPR active. The most distinct feature is that the EPR spectra are easily obtained at ambient temperatures, characteristic of $d^1$ systems ($Mo^V$). The reaction product from the treatment of $H_3$(tpfc) with $SbCl_3$ was isolated in a 95% yield as the pyridine-coordinated antimony(III) corrole **2a**, with the $^{19}F$ and $^1H$ NMR spectra revealing the symmetry and coordinated pyridine molecules, respectively. The (oxo)-antimony(V) corrole **2b** was obtained in quantitative yields by either slow aerobic or fast chemical oxidation of **2a**, accompanied by a color change from green to red and changes in the $^{19}F$ NMR spectrum that are consistent with $C_s$ symmetry. Treatment of either **2a** or **b** with aqueous HF (48%) led to the *trans*-difluoroantimony(V) complex **2c** in a 97% isolated yield, for which the coordinated F ligands are clearly evident in the $^{19}F$ NMR spectrum. These reactions are summarized in Scheme 1.

(3) Gross, Z.; Gray, H. B. *Adv. Synth. Catal.* **2004,** 346, 165–170.
(4) Meier-Callahan, A. E.; Gray, H. B.; Gross, Z. *Inorg. Chem.* **2000**, *39*, 3605–3607. (b) Meier-Callahan, A. E.; Di Bilio, A. J.; Simkhovich, L.; Mahammed, A.; Goldberg, I.; Gray, H. B.; Gross, Z. *Inorg. Chem.* **2001**, *40*, 6788–6793.
(5) Mahammed, A.; Gray, H. B.; Meier-Callahan, A. E.; Gross, Z. *J. Am. Chem. Soc.* **2003**, *125*, 1162–1163.
(6) Groves, J. T.; Quinn, R. *J. Am. Chem. Soc.* **1985**, *107*, 5790. (b) Groves, J. T.; Ahn, K.-H.; Quinn, R. *J. Am. Chem. Soc.* **1988**, *110*, 4217. (c) Groves, J. T.; Bonchio, M.; Carofiglio, T.; Shalyaev, K. *J. Am. Chem. Soc.* **1996**, *118*, 8961.
(7) Simkhovich, L.; Luobeznova, I.; Goldberg, I.; Gross, Z. *Chem.—Eur. J.* **2003**, *9*, 201–208. (b) Jerome, F.; Billier, B.; Barbe, J. M.; Espinosa, E.; Dahaoui, S.; Lecomte, C.; Guilard, R. *Angew. Chem., Int. Ed.* **2000**, *39*, 4051–4053.
(8) Fujihara, T.; Hoshiba, K.; Sasaki, Y.; Imamura, T. *Bull. Chem. Soc. Jpn.* **2000**, *73*, 383–390. (b) Liu, W.-S.; Zhang, R.; Huang, J.-S.; Che, C.-M.; Peng, S.-M. *J. Organomet. Chem.* **2001**, *634*, 34–38. (c) Ledon, H. J.; Durbut, P.; Varescon, F. *J. Am. Chem. Soc.* **1981**, *103*, 3601–3603. (d) Hoffmann, P.; Meunier, B. *New. J. Chem.* **1992**, *16*, 559–561. (e) Brand, H.; Arnold, J. *Coord. Chem. Rev.* **1995**, *140*, 137–168.
(9) Weber, L.; Haufe, G.; Rehorek, D.; Hennig, H. *J. Mol. Catal.* **1990**, *60*, 267–271. (b) Inoue, H.; Okamoto, T.; Kameo, Y.; Sumitani, M.; Fujiwara, A.; Ishibashi, D.; Hida, M. *J. Chem. Soc., Perkin Trans. 1* **1994**, 105–111. (c) Shiragami, T.; Kubomura, K.; Ishibashi, D.; Inoue, H. *J. Am. Chem. Soc.* **1996**, *118*, 6311–6312. (d) Shiragami, T.; Shimizu, Y.; Hinoue, K.; Fueta, Y.; Nobuhara, K.; Akazaki, I.; Yasuda, M. *J. Photochem. Photobiol. A* **2003**, *156*, 115–119. (e) Takagi, S.; Suzuki, M.; Shiragami, T.; Inoue, H. *J. Am. Chem. Soc.* **1997**, *119*, 8712–8713. (f) Knor, G. *ChemBioChem* **2001**, *2*, 593–596.
(10) Murakami, Y.; Matsuda, Y.; Yamada, S. *Chem. Lett.* **1977**, 689–692. (b) Sashuk, V.; Koszarna, B.; Winiarek, P.; Gryko, D. T.; Grela, K. *Inorg. Chem. Commun.* **2004**, *7*, 871–875.
(11) Kadish, K. M.; Erben, C.; Ou, Z. P.; Adamian, V. A.; Will, S.; Vogel, E. *Inorg. Chem.* **2000**, *39*, 3312–3319.

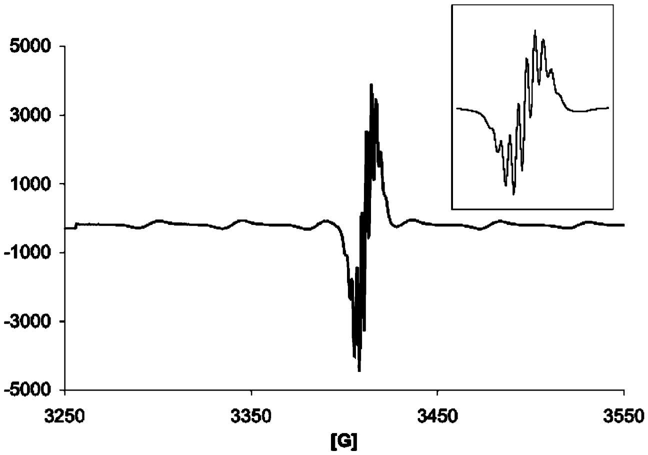


**Figure 1.** EPR spectrum of the (oxo)molybdenum(V) corrole **1b** ($A^{14}{}_{N}$ = 0.27 mT, $A^{97}{}_{Mo}$ = 4.68 mT, $g$ = 1.975) in benzene at room temperature. Inset: Enlargement of the central feature.

**Spectroscopy.** The main spectroscopic tool for the characterization of the (oxo)molybdenum(V) corroles was EPR, relying on the fact that only $d^1$ metal complexes provide high-resolution spectra at room temperature. The spectra of **1a** and **b** (Figure 1) met this expectation and were quite revealing indeed: large hyperfine splitting from Mo ($A^{97}{}_{Mo}$ = 4.66 mT for **1a** and 4.68 mT for **1b**) and smaller yet well resolved superhyperfine splitting from the four N atoms of the coordinated corrole trianion ($A^{14}{}_{N}$ = 0.257 mT for **1a** and 0.266 mT for **1b**). The coupling constants in **1a** and **b** are qualitatively similar to those reported for (oxo)molybdenum(V) complexes of a very different corrole and of porphyrins.[12,13] A comparison with the other (oxo)molybdenum(V) triarylcorroles is not possible[10b] because hyperfine splitting constants were not reported and superhyperfine splitting were not resolved in that investigation. Nevertheless, the smaller $A^{97}{}_{Mo}$ and $A^{14}{}_{N}$ values in **1a** relative to **1b** indicate that the former has significantly less unpaired spin density on both the N atoms and the metal ion than the latter. This may be attributed to the more electron-withdrawing $C_6F_5$ groups on the *meso*-C atoms of the corrole in **1a** relative to the less electron-withdrawing $C_6H_3Cl_2$ substituents in **1b**. In contrast with the previous report,[10b] the electronic spectrum of **1a** is not different from those of the other (oxo)molybdenum(V) triarylcorroles (including **1b**) which display sharp red-shifted Soret bands with maxima above 435 nm.

For the diamagnetic antimony corroles, NMR spectroscopy was the main tool for quite detailed structural determination. In all cases, the four $\beta$-pyrrole doublets with two different $J$ coupling constants that are apparent in the $^1$H NMR spectra (Figure 2a−c) and the clear separation of *ortho*-, *meta*-, and para-F atoms at about −137, −164, and −151 ppm, respectively, in the $^{19}$F spectra (Figure 3a−c) confirm that no dramatic structural or electronic changes took place upon metal insertion.[14] The more in-depth analysis allowed for quite detailed conclusions about the structures of the complexes.

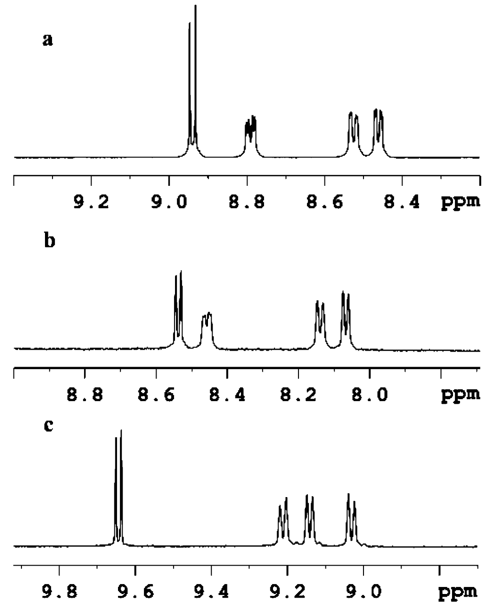


**Figure 2.** $^1$H NMR spectra (300 MHz, benzene-$d_6$) of the (a) antimony(III), (b) (oxo)antimony(V), and (c) difluoroantimony(V) corroles **2a**−**c**. Note the additional couplings by the F atoms, most apparent in the top spectrum.

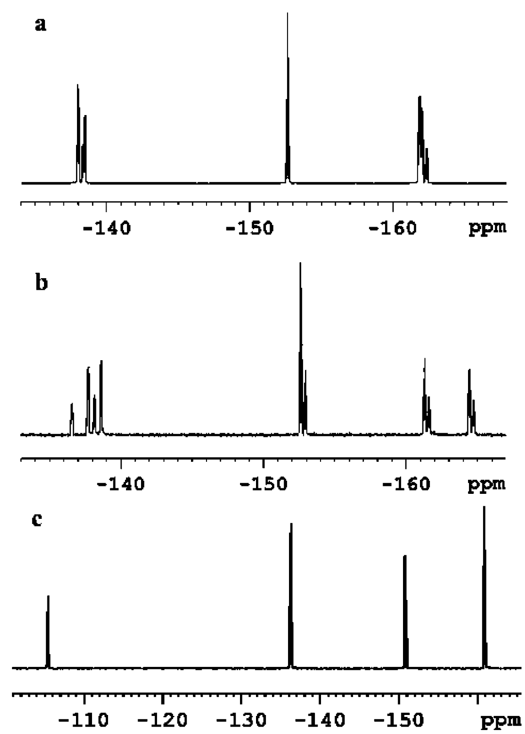


**Figure 3.** $^{19}$F NMR spectra of the (a) antimony(III), (b) (oxo)antimony(V), and (c) difluoroantimony(V) corroles **2a**−**c**, in benzene-$d_6$.

Complex **2a** was prepared in pyridine, and the crystallization solvent mixture also contained pyridine, a procedure that leads to bis-pyridine complexes with many other metallocorroles.[15] The MS spectrum of **2a** displayed only the noncoordinated metallocorrole, which is a common phenomenon. However, the $^{19}$F NMR spectrum (Figure 3a)

(12) Matsuda, Y.; Yamada, S.; Murakami, Y. *Inorg. Chem.* **1981**, *20*, 2239−2246.
(13) Ledon, H. J.; Bonnet, M. C.; Brigandat, Y.; Varescon, F. *Inorg. Chem.* **1980**, *19*, 3488−3491.
(14) Balazs, Y S.; Saltsman, I.; Mahammed, A.; Tkachenko, E.; Golubkov, G.; Levine, J.; Gross, Z. *Magn. Reson. Chem*. **2004**, *42*, 624−635.

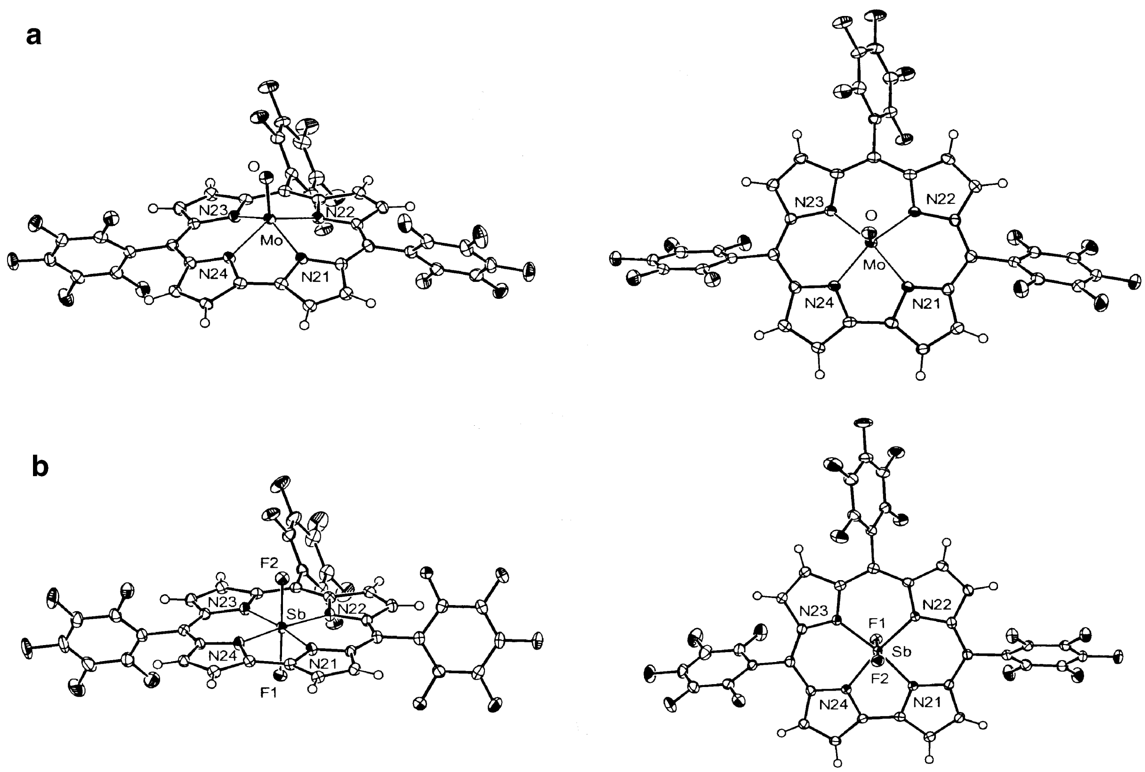


**Figure 4.** (a) Molecular structure of **1a**, showing 50% probability thermal displacement parameters at ca. 110 K. The bond lengths around the Mo center are as follows: Mo═O = 1.684(2) Å, Mo−N range = 2.033−2.039(2) Å. Note the domed conformation. (b) Molecular structure of **2c**, showing 50% probability thermal displacement parameters at ca. 110 K. The bond lengths around the Sb center are as follows: Sb−F1 = 1.940(1) Å, Sb−F2 = 1.932(1) Å, Sb−N(pyrrole) range = 1.971−1.979(2) Å. The corrole core ring is essentially planar.

displays four signals for the *ortho*-F atoms in a 1:2:1:2 integration ratio at around −138 ppm. This is clearly inconsistent with any symmetry element that would turn the below- and above-plane *ortho*- and *meta*-F atoms identical, thus ruling out the $C_{2v}$ symmetry of both the noncoordinated (MS data) and bis-pyridine-coordinated (synthetic expectations) antimony corrole. This conclusion is not limited to benzene-$d_6$ solutions, as similar spectra were obtained in $CD_3$-CN and even in pyridine-$d_5$. Resolution of this apparent conflict comes from $^1$H NMR spectroscopy where sharp signals characteristic of pyridine molecules were obtained at chemical shifts that varied from one batch to the other and even on the concentration of the sample. In general, the chemical shifts were between those expected of the free and metal-coordinated pyridine, showing that the coordination of pyridine to **2a** is reversible and fast on the NMR time scale. The conclusion that the dominant species in solution is five-coordinate (i.e, an antimony(III) corrole with only one pyridine ligated to the axial position) is consistent with both the $^1$H and $^{19}$F NMR data. All together, the affinity of **2a** to pyridine is apparently much smaller than of other metallocorroles (i.e., the Lewis acidity of the antimony(III) corrole is quite low). This phenomenon is apparently the result of the "inert pair effect" of the $d^{10}s^2$ ion,[16] which is stereochemically active and hence disfavors coordination of pyridine as the sixth ligand.

For **2b**, the MS spectrum displayed a 100% intensity signal with the expected *m*/*z* for the (oxo)antimony(V) corrole (tpfc)Sb(O). The $^{19}$F NMR spectrum (Figure 3b), displaying two *ortho*-F and two *meta*-F resonances for each of the individual $C_6F_5$ rings, was the most distinctive evidence for penta coordination ($C_s$ symmetry). For example, values of −136.55 and −138.12 ppm for *ortho*-F and −161.67 and −164.77 ppm for *meta*-F were obtained for the unique $C_6F_5$ group (on C10 of the corrole) because of the syn and anti relationships of these atoms relative to the Sb═O moiety. Upon transformation of **2b** to the *trans*-difluoro complex **2c**, the increase in symmetry to $C_{2v}$ is easily recognized by the decreased number of signals for the $C_6F_5$ rings (between −136 and −161 ppm) in the $^{19}$F NMR spectrum (Figure 3c). In addition, the antimony-coordinated F atoms appear as one singlet at a very different field (−105.4 ppm). The MS spectrum of **2b** displayed a 100% intensity signal with an *m*/*z* consistent with the *trans*-difluoroantimony corrole (tpfc)-Sb(F)$_2$.

**X-ray Crystallography.** ORTEP plots of **1a** and **2c**, shown in Figure 4, represent rather precise structural determinations of the two compounds. The 5-coordinate corrole **1a** adopts a domed structure, as the molybdenum(V) ion is pulled out of the ring center toward the axial O.

(15) Mahammed, A.; Giladi, I.; Goldberg, I.; Gross, Z. *Chem.*−*Eur. J.* **2001**, *7*, 4259. (b) Bendix, J.; Dmochowski, I. J.; Gray, H. B.; Mahammed, A.; Simkhovich, L.; Gross, Z. *Angew. Chem., Int. Ed.* **2000,** *39*, 4048. (c) Weaver, J. J.; Sorasaenee, K.; Sheikh, M.; Goldschmidt, R.; Tkachenko, E.; Gross, Z.; Gray, H. B. *J. Porphyrins Phthalocyanines* **2004**, *8*, 76−81.

(16) Couch, D. A.; Wilkins, C. J.; Rossman, G. R.; Gray, H. B. *J. Am. Chem. Soc.* **1970**, *92*, 307−310. (b) Knor, G.; Vogler, A. *Inorg. Chem.* **1994**, *33*, 314−318

The metal ion lies 0.729(1) Å above the mean plane of the four pyrrole N atoms. Optimization of the pyramidal coordination around Mo is associated with different twisting of the pyrrole rings with respect to the $N_4$ plane, the N21 and N24 pyrrole rings being characterized by the largest "doming" effect. The corresponding twist angles are 16.3, 4.4, 8.6, and 15.5(2)° for the N21, N22, N23, and N24 pyrroles, respectively. This places the pyrrole N atoms 0.314−0.506(2) Å above the mean plane defined by the four peripheral C−C bonds of the pyrrole rings. In the crystal, a molecule of the benzene solvent lies parallel, and in close vicinity, to the concave face of the pyrrole macrocycle. The observed Mo═O and Mo−N bond lengths are comparable to those observed earlier for five-coordinate (oxo)molybdenum complexes with porphyrin and phthalocyanine macrocycles.[17]

The corrole ring of the 6-coordinate complex **2c** is nearly planar. The deviations of the individual carbon atoms from the mean plane of the 19-membered C framework are within −0.09 to +0.06 Å, with an rms deviation of 0.04 Å. The Sb(V) ion lies in the center of the core ring and is coplanar with the pyrrole N-atoms, and therefore, the Sb−N distances are shorter than the Mo(V)−N ones in **1a**, despite its larger size. To our knowledge, only a single structure of an antimony−porphyrinoid complex has been determined thus far, involving the tetraphenylporphyrin−Sb(F)(Me)$^+$ moiety.[18] While, in relation to the present observations, the latter reveals a comparable Sb−F bond length (1.928 Å), it also shows considerably longer Sb−N(pyrrole) distances (within 2.087−2.115 Å). This should be attributed to the slight deviation of the Sb ion placed in an axially asymmetric (octahedral) coordination environment from the porphyrin core toward the F ligand, as well as to the somewhat contracted inner cavity in the 23-membered corrole moiety (in this study) than in the 24-membered porphyrin macrocycle.

**Electrochemistry.** The cyclic voltammograms of the two (oxo)molybdenum(V) corroles revealed $E_{1/2}$ values of −0.35 and 1.32 V for **1a** and −0.49 and 1.04 V for **1b**, which may be compared with the $E_{1/2}$ values (−0.70 and + 0.72 V) obtained for an analogous complex with a much more electron-rich corrole [(mec)Mo(O), where mec stands for the trianion of 2,3,17,18-tetramethyl-7,8,12,13-tetraethylcorrole].[12] As corrole-centered reductions were repeatedly shown to require very negative potentials (<−1 V),[2h,19] the relatively low reduction potentials of **1a** and **b** may safely be assigned to metal-centered processes. The redox potentials of >1 V could be consistent with either metal- or corrole-centered oxidations, but the latter option is more consistent with the following data. The effect of the *meso*-$C_6F_5$ substituent in **1a** versus *meso*-$C_6H_3Cl_2$ in **1b** on the oxidation potential is much larger than on the metal-centered reduction: 0.28 versus 0.14 V, respectively. Spectroscopic examination of the chemical oxidation of **1b** by $[Ar_3N]^+SbCl_6^-$ (Ar = 4-bromophenyl, $E_{1/2}$ = 1.1 V) revealed a disappearance of the EPR signal without a buildup of a NMR spectrum, consistent with expectation for (corrole radical)molybdenum(V) and inconsistent with molybdenum(VI). Another revealing comparison is between **1a** and the analogous (oxo)chromium(V) complex (tpfc)Cr(O), for which the $E_{1/2}$ values of 0.11 and 1.24 V were shown to reflect metal- and corrole-based redox processes, respectively.[4b] The almost identical oxidation potentials are supportive of a corrole-centered oxidation in both cases, showing that the (oxo)molybdenum(VI) oxidation state is not accessible by one-electron oxidation of **1a**. Finally, the 0.46 V difference between the (corrolato)$Mo^V$(O)/[(corrolato)$Mo^{IV}$(O)]$^-$ and (corrolato)$Cr^V$(O)/[(corrolato)$Cr^{IV}$(O)]$^-$ redox couples leads to the expectation of **1a** being an even less reactive oxidation catalyst than (tpfc)Cr(O).

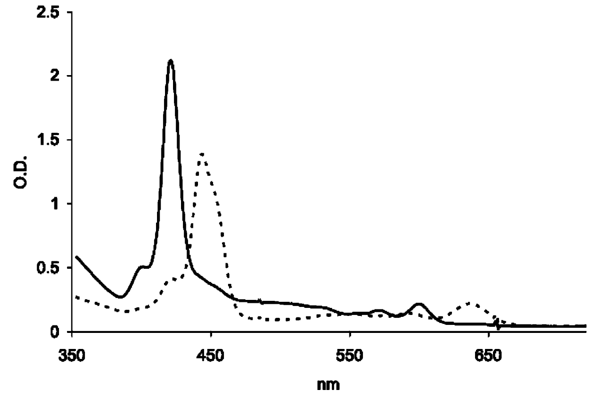


**Figure 5.** Electronic spectra of the antimony(III) corrole **2a** before (broken line) and after (full line) the addition of the $[Ar_3N^{+\cdot}]SbCl_6^-$ oxidant.

The antimony(III) corrole **2a** displayed two redox potentials of which the one with $E_{1/2}$ = −1.1 V necessarily reflects reduction of the corrole. Assignment of the redox process with $E_{1/2}$ = 1.0 V to either an antimony(III)/antimony(IV) process or oxidation of the corrole is not as obvious. On one hand, oxidation of the metal was proposed to precede that of the corrole in the antimony(III) complex of an electron-rich corrole.[11] Indeed, spectroscopic examination of the chemical oxidation of **2a** by$[Ar_3N]^+SbCl_6^-$ (Figure 5) revealed a change from a hyper ($\lambda_{max}$ = 444 nm) to a normal ($\lambda_{max}$ = 421 nm) spectrum that is consistent with oxidation to antimony(IV). On the other hand, the 2.1 V difference between the two redox couples in **2a** is consistent with both processes being corrole-centered as it fits perfectly within the HOMO−LUMO gap of 2.12 ± 0.02 V determined for triarylcorroles (and 2.25 ± 0.15 V for a larger range of corroles).[2h,19] An intriguing possibility that would be consistent with all the data, of precedence in both corrole and porphyrin chemistry,[19,20] is conversion of an initially formed corrole-oxidized antimony(III) into antimony(IV) corrole. No such ambiguity exists for the antimony(V) corroles **2b** and **c**, where the oxidation potentials reflect oxidation of the

(17) Borchel, V.; Strahle, J. *Z. Naturforsch. B* **1984**, *39*, 1664. (b) Janczak, J.; Kubiak, R. *Inorg. Chem.* **1999**, *38*, 2429−2433. (c) Jacoby, D.; Floriani, C.; Chiesi-Villa, A.; Rizzoli, C. *Chem. Commun.* **1991**, 220. (d) Hamstra, B. J.; Cheng, B.; Ellison, M. K.; Scheidt, W. R. *Inorg. Chem.* **1999**, *38*, 3554−3561.

(18) Kadish, K. M.; Autret, M.; Ou, Z.; Akiba, K.; Masumoto, S.; Wada, R.; Yamamoto, Y. *Inorg. Chem.* **1996**, *35*, 5564−5569.

(19) Kadish, K. M.; Ou, Z. P.; Adamian, V. A.; Guilard, R.; Gros, C. P.; Erben, C.; Will, S.; Vogel, E. *Inorg. Chem.* **2000**, *39*, 5675−5682.

(20) Groves, J. T.; Gross, Z.; Stern, M. K. *Inorg. Chem.* **1994**, *33*, 5065−5072.

corrole. The vast differences between the $E_{1/2}$ values (1.10 and 1.47 V for **2b** and **c**, respectively) reveal that the $[Sb(F)_2]^{3+}$ moiety is much more electron withdrawing than $[Sb(O)]^{3+}$. This effect is less dominant in the reduction process, for which smaller differences ($E_{1/2} = -0.77$ and $-0.64$ V for **2b** and **c**, respectively) were obtained.

**Chemical Oxidations/Reductions.** Since the electrochemical results suggested that molybdenum(VI) is not accessible for these corroles, the focus was toward affecting the chemical reduction of the (oxo)molybdenum(V) corroles **1a** and **b** to molybdenum(III). This included reactions with trisubstituted phosphines and a variety of reducing agents (Zn, hydrazine, $NaBH_4$). Treatment of **1a** or **b** with triphenylphosphine, which worked well for oxygen-atom transfer-based reduction of (tpfc)Cr(O) to the chromium(III) corrole (tpfc)Cr, revealed that no reaction took place. This is consistent with the significantly more negative reduction potentials of (oxo)molybdenum(V) than those of (oxo)-chromium(V) corroles. The use of the much more oxophilic triethylphosphine revealed that it reacted with **1a** and **b**, but only the corresponding metal-free corroles could be isolated. An identical phenomenon occurred with all other reagents (i.e., either no reaction or demetalation). Attempts to interfere with the apparently facile demetalation of the initial reaction product included using a large excess of triethylphosphine or amines (pyridine and imidazole) for coordinating the molybdenum(III) corroles. Unfortunately, all of these attempts were not successful.

The conversion of the antimony(III) corrole **2a** into the (oxo)antimony(V) corrole **2b** could be accomplished by treatment with either chemical oxidants (almost immediate reaction) or molecular oxygen (30 min at reflux and days at RT). The reverse reaction took place when **2b** was treated with triphenylphoshine overnight at room temperature under Ar. Importantly, the antimony(V) corroles **2b** and **c** were not reduced to **2a** via treatment by the olefins and alkanes that were used as substrates in the catalytic reactions. Thioanisole reduced **2b** (but not **2c**), but at rates (2 h at reflux were required for completion) that were much too slow to account for the catalytic reactions.

**Reactivity as Catalysts.** Screening reactions to determine if the antimony corroles are useful catalysts for the photo-assisted aerobic oxidation of thioanisole were performed in three solvents. The results, displayed in entries 1−9 of Table 1, revealed a very significant solvent effect. There was no reaction in benzene (entries 1−3), and reactions performed in acetonitrile (entries 4−6) were limited and catalyst-dependent: 0, 3, and 11% conversion with catalysts **2a**, **b**, and **c**, respectively. In contrast, full conversion of thioanisole to the corresponding sulfoxide was obtained in ethanol (and other alcohols, not shown), regardless of the catalyst used (entries 7−9). There were no organic byproducts in these and all other reactions, including further oxidation of the sulfoxide to the corresponding sulfone. The control reactions (entries 10−16) clearly emphasized the need for both the catalyst and irradiation, as the sulfide was not oxidized when either of these was omitted. When molecular oxygen was replaced with air, the efficiency was reduced from 100 to 2−10% conversion (entries 14−16). The superiority of **2c** as catalyst relative to **2b** and of the latter relative to **2a**, already apparent in the results obtained in acetonitrile (entries 4−6) and those with air rather than oxygen (entries 14−16), reappeared in reactions in which the substrate was more concentrated (entries 17−19). Only catalyst **2c** provided the optimal 5000 catalytic turnovers and remained unchanged at the end. The color changes during reactions catalyzed by **2a** and **2b** signaled the oxidation of the former (green) to the latter (red) early on, as well as the reduction of **2b** to **2a** and the formation of another green complex toward the end. The same order of catalytic efficiency (**2c** > **2b** > **2a**) was obtained when the formation of the oxidation product, methylphenylsulfoxide, was examined as a function of reaction time (Figure 6). Finally, there was no reaction when thioanisole was replaced by diphenylsulfide. The latter substrate was specifically chosen because it is known to be inert toward oxidation by singlet oxygen.[21]

Complex **2c** was further examined as a potential photocatalyst for the oxidation of hydrocarbons. The screening reactions (Table 2, entries 1−6) revealed an absolute selectivity toward CH versus C═C bonds: styrene remained

**Table 1.** Aerobic Oxidation of Thioanisole (S) to the Corresponding Sulfoxide (SO), with Antimony(III), (Oxo)antimony(V), and Difluoroantimony(V) Corroles (**2a**, **b**, and **c**, respectively) as Photocatalysts

| entry | solvent | catalyst | reaction conditions[a] | substrate/cat (mol/mol) | SO/S (%) | TON[e] |
|---|---|---|---|---|---|---|
| | | | screening reactions | | | |
| 1 | $C_6H_6$ | **2a** | $O_2$, h$\nu$ | 1000:1 | 0:100 | 0 |
| 2 | $C_6H_6$ | **2b** | $O_2$, h$\nu$ | 1000:1 | 0:100 | 0 |
| 3 | $C_6H_6$ | **2c** | $O_2$, h$\nu$ | 1000:1 | 0:100 | 1000 |
| 4 | $CH_3CN$ | **2a** | $O_2$, h$\nu$ | 1000:1 | 0:100 | 1000 |
| 5 | $CH_3CN$ | **2b** | $O_2$, h$\nu$ | 1000:1 | 3:97 | 30 |
| 6 | $CH_3CN$ | **2c** | $O_2$, h$\nu$ | 1000:1 | 11:89 | 110 |
| 7 | EtOH | **2a**[b] | $O_2$, h$\nu$ | 1000:1 | 100:0 | 1000 |
| 8 | EtOH | **2b** | $O_2$, h$\nu$ | 1000:1 | 100:0 | 1000 |
| 9 | EtOH | **2c** | $O_2$, h$\nu$ | 1000:1 | 100:0 | 1000 |
| | | | control reactions | | | |
| 10 | EtOH | none | $O_2$, h$\nu$ | 100:0 | 0:100 | 0 |
| 11 | EtOH | **2a** | $O_2$, heat | 100:1 | 0:100 | 0 |
| 12 | EtOH | **2b** | $O_2$, heat | 100:1 | 0:100 | 0 |
| 13 | EtOH | **2c** | $O_2$, heat | 100:1 | 0:100 | 0 |
| 14 | EtOH | **2a** | air, h$\nu$ | 100:1 | 2:98 | 2 |
| 15 | EtOH | **2b** | air, h$\nu$ | 100:1 | 4:96 | 4 |
| 16 | EtOH | **2c** | air, h$\nu$ | 100:1 | 10:90 | 10 |
| | | | high-turnover reactions | | | |
| 17 | EtOH | **2a**[b,c] | $O_2$, h$\nu$ | 5000:1 | 81:19 | 4050 |
| 18 | EtOH | **2b**[d] | $O_2$, h$\nu$ | 5000:1 | 90:10 | 4500 |
| 19 | EtOH | **2c** | $O_2$, h$\nu$ | 5000:1 | 100:0 | 5000 |

[a] General reaction conditions: 2 h reflux (heat supplied from either the lamp or external source) of solutions composed of thioanisole [0.12 mL (1 mmol) in entries 1−9, 0.012 mL (0.1 mmol) in entries 10−16, 0.59 mL (5 mmol) in entries 17−19] in 20 mL solvent, with a sunlight lamp (230 W, Osram) placed 10 cm from the bottom of a 50 mL round-bottom Pyrex flask. [b] After 5 min, the color of the reaction mixture changed from green to red, and it returned to green after 1.5 h. TLC examinations revealed that the color changes were the result of the conversions of **2a** to **2b** and back to **2a**. [c] A new compound (not characterized) also appeared on the TLC, remaining on the baseline. [d] After 1.5 h, the color of mixture changed from red to dark green. TLC examinations revealed that **2b** was partially converted to **2a** and to a new compound that remained on the baseline. [c] TON = turnover numbers (i.e., (mol product)/(mol catalyst)).

(21) Bonesi, S. M.; Fagnoni, M.; Monti, S.; Albini, A. *Photochem. Photobiol. Sci.* **2004**, *3*, 489−493.

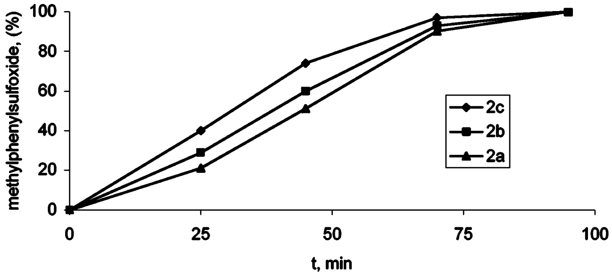


**Figure 6.** Time-dependent formation of methylphenylsulfoxide during oxygenation of thioanisole with 0.1 mol % of the various antimony corroles as photocatalysts.

**Table 2.** Aerobic Oxidation of Hydrocarbons (S) to the Corresponding Hydroperoxides (SO) with the Difluoroantimony(V) Corrole **2c** as the Photocatalyst

| entry | hydrocarbon | reaction conditions[a] | substrate/cat (mol/mol) | SO/S (%) | TON[b] |
|---|---|---|---|---|---|
| | | screening reactions | | | |
| 1 | cyclohexene | $O_2$, h$\nu$, 7 h | 1000:1 | 100:0 | 1000 |
| 2 | cyclooctene | $O_2$, h$\nu$, 8 h | 1000:1 | 100:0 | 1000 |
| 3 | styrene | $O_2$, h$\nu$, 7 h | 500:1 | 0:100 | 0 |
| 4 | ethylbenzene | $O_2$, h$\nu$, 7 h | 500:1 | 0:100 | 0 |
| 5 | cumene | $O_2$, h$\nu$, 7 h | 500:1 | 100:0 | 500 |
| 6 | adamantane | $O_2$, h$\nu$, 10 h | 500:1 | 0:100 | 0 |
| | | control reactions | | | |
| 10 | cyclohexene | $O_2$, h$\nu$, no catalyst | 1000:0 | 0:100 | 0 |
| 11 | cyclohexene | $O_2$, heat, 7 h | 1000:1 | 0:100 | 0 |
| 12 | cyclohexene | air, h$\nu$, 7 h | 1000:1 | 7:93 | 70 |
| 13 | cyclooctene | $O_2$, heat, 8 h | 1000:1 | 0:100 | 0 |
| 14 | cyclooctene | air, h$\nu$, 8 h | 1000:1 | 0:100 | 0 |
| 15 | cumene | $O_2$, heat, 8 h | 1000:1 | 5:95 | 50 |
| 16 | cumene | air, h$\nu$, 8 h | 1000:1 | 0:100 | 0 |
| | | higher-turnover reactions | | | |
| 17 | cyclohexene | $O_2$, h$\nu$, 10 h | 2000:1 | 78:22 | 1560 |
| 18 | cyclooctene | $O_2$, h$\nu$, 10 h | 2000:1 | 67:33 | 1340 |
| 19 | cumene | $O_2$, h$\nu$, 12 h | 1000:1 | 60:40 | 600 |

[a] General reaction conditions: reflux (heat supplied from either the lamp or external source) of solutions composed of catalyst **2c** (1 mg, 1 $\mu$mol), hydrocarbon [1 mmol in entries 1, 2, and 10−16; 0.5 mmol in entries 3−6; 2 mmol in entries 17−19] in 20 mL ethanol with a sunlight lamp (230 W, Osram) placed 10 cm from the bottom of a 50 mL round-bottom Pyrex flask. [b] TON = turnover numbers (i.e., (mol product)/(mol catalyst)).

unreacted and only the allylic CH bonds of cyclohexene and cyclooctene were oxidized. This fits the reactivity profile of singlet oxygen, which is characterized by very efficient “ene” reactions.[22] Of the three non-olefin-containing substrates that were examined, only cumene (not ethylbenzene or admantane) was oxidized. These results are also consistent with singlet oxygen as the oxidizing reagent, with the selectivity reflecting the mechanistic aspects of reactions that proceed with C−H abstraction as the rate-limiting step.[23] The control reactions (Table 2, entries 10−16) also show that there is no reaction of any of the substrates when any of the constituents required for efficient formation of singlet oxygen is omitted. Another aspect of selectivity is that single products, the corresponding hydroperoxides, were obtained in all cases. This conclusion is based on $^1$H NMR analysis of reaction mixtures, performed by dissolving aliquots from the untreated (without solvent evaporation or any other

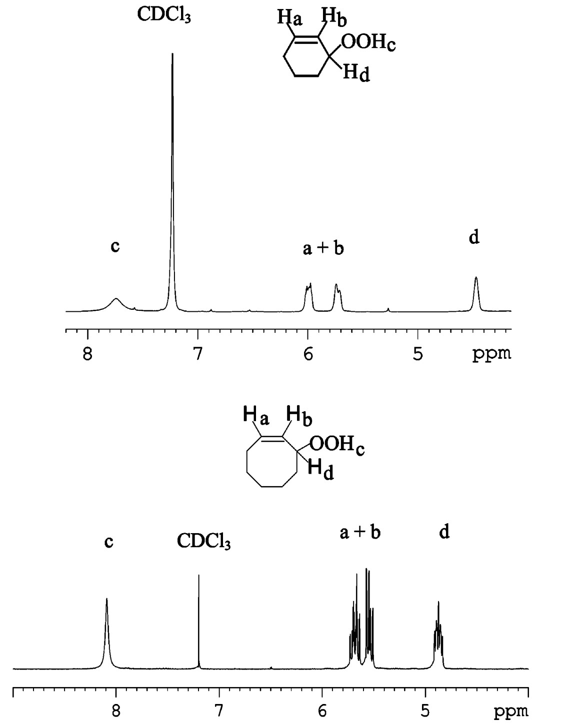


**Figure 7.** $^1$H NMR analysis (in $CDCl_3$) of ethanolic solutions that initially contained 50 mM hydrocarbon and 0.05 mM **2c**, recorded for the reactions of cyclohexene (top) and cyclooctene (bottom), 7 and 8 h, respectively, after the sunlamp was turned on.

workup procedure) reaction mixtures in $CDCl_3$. The results for cyclohexene and cyclooctene are shown in Figure 7. In both cases, the vinylic and allylic CH resonances were located at lower field than in the analogous alcohols (2-cyclohexene-1-ol and 2-cyclooctene-ol, respectively), consistent with CH−OOH rather than CH−OH moieties. In addition, the NMR spectrum of the cumene product and commercially available cumene hydroperoxide were found to be identical. In all three cases, the signals from the CH−OOH moieties changed cleanly and quantitatively to those of the corresponding alcohols upon addition of triphenylphosphine. Finally, when the ratio of substrate to catalyst was increased to 2000:1, up to 78% conversion was obtained (Table 2, entries 17−19), and catalyst **2c** was not destroyed or modified to any appreciable extent (TLC and UV−vis examinations). To the best of our knowledge, these results are better than all previous reports in terms of absolute catalytic turnover numbers and selectivity.[24]

## Conclusions

Two molybdenum (one new) and three new antimony corroles were isolated and thoroughly characterized. The crystal structure of the (oxo)molybdenum(V) corrole **1a** is the first of it kind, revealing that the metal ion is displaced far above the corrole. The very negative reduction potentials of the (oxo)molybdenum(V) corroles are clearly related to their inactivity as oxygen transfer reagents. The crystal structure of the *trans*-difluoroantimony(V) corrole **2c**, the first of it kind in both corroles and porphyrins, reveals a

(22) Kearns, D. R. *Chem. Rev.* **1971**, *71*, 395−427.
(23) Bryant, J. R.; Mayer, J. M. *J. Am. Chem. Soc.* **2003**, *125*, 10351−10361.
(24) Zen, J. M.; Liou, S. L.; Kumar, A. S.; Hsia, M. S. *Angew. Chem., Int. Ed.* **2003**, *42*, 577−579 and references therein.

very planar corrole ring, short Sb−F bonds, and long Sb−N(pyrrole) distances. All three antimony corroles displayed high activity as catalysts for photoinduced oxidation of thioanisole by molecular oxygen, with superior results obtained in alcoholic solvents. Allylic and some benzylic CH bonds were also oxidized under those conditions, with absolute selectivity to the corresponding hydroperoxides. In all cases, the catalytic performances were in the order of **2a** < **b** < **c**, in parallel with the lifetimes of the excited triplet states.[25] All evidence points toward singlet oxygen as the sole oxidant in these reactions.

## Experimental Section

**Physical Methods.** The $^1$H and $^{19}$F NMR spectra were recorded on either a Bruker AM 200, operating at 200 MHz for $^1$H NMR and 188 MHz for $^{19}$F NMR, or a Bruker AM 300, operating at 300 MHz for $^1$H NMR and 282 MHz for $^{19}$F NMR. Chemical shifts are reported in ppm relative to residual hydrogen atoms in the deuterated solvents (7.24; 7.15; and 8.59, 7.62, and 7.23 for chloroform, benzene, and pyridine, respectively) for the $^1$H NMR spectra and relative to $CFCl_3$ ($\delta$ = 0.00) in the $^{19}$F NMR. The electronic spectra were recorded on a HP 8452A diode array spectrophotometer and gas chromatographic analysis was performed on a HP-5890 GC equipped with a HP-5 capillary column and FID detector. The redox potentials were determined by cyclic voltammetry (CV) at ambient temperatures on a homemade voltammograph, using $CH_2Cl_2$ or $CH_3CN$ solutions, 0.05 M *n*-tetrabutylammonium perchlorate (TBAP, Fluka, recrystallized three times from absolute ethanol), and about 0.5 mM in substrate. The reference electrode was Ag/AgCl. EPR spectra were recorded on a Bruker EMX-10/12 X-band digital EPR spectrometer equipped with a Bruker $N_2$-temperature controller. MS analysis was performed on a Micromass MS Technologies Maldi micro MX with ionization by a nitrogen laser at 337 nm. The other experimental conditions are reported in the legends of the corresponding spectra.

**Materials.** Dichloromethane (Bio-Lab LTD), pyridine (Merck), ethanol (Bio-Lab LTD), *n*-heptane (Carlo-Erba), *n*-hexane (Bio-Lab LTD), $SbCl_3$ (Aldrich), benzene (Aldrich), Decaline (Riedel-de Haen), $Mo(CO)_6$ (Merck), and deuterated solvents (Aldrich and Cambridge Isotopes products) were used as received.

**Synthetic Methods.** The synthetic details for the preparation of $H_3$(tpfc) and $H_3$(tdcc) are provided in previous publications.[1]

**Molybdenum Corroles. (5,10,15-Trispentafluorophenylcorrolato)(oxo)molybdenum(V) (1a).** A solution of $H_3$(tpfc) (50 mg, 0.06 mmol) in Decalin (50 mL) was heated to 170−180 °C, followed by the addition of $Mo(CO)_6$ (0.073gr, 0.3 mmol). TLC examinations (silica gel, *n*-hexane/$CH_2Cl_2$ = 2:1) revealed that the starting material was fully consumed within 1 h of reaction, after which the solvent was evaporated. Crystallization from a benzene/*n*-hexane mixture yielded 39.6 mg (73%) of dark red X-ray quality crystals of (tpfc)Mo(O), **1a**.

UV−vis ($CH_2Cl_2$, $\lambda_{max}$ ($\epsilon \times 10^{-4}$)): 434 (11.49), 508 (0.42), 546 (1.30), 578 nm (1.76). MS (DCI$^-$): *m/z* 907 ([M$^-$], 100%). EPR ($CH_2Cl_2$, room temperature): $g$ = 1.975, $A^{14}{}_{N}$ = 0.257 mT, $A^{97}{}_{Mo}$ = 4.66 mT. Electrochemistry: $E_{1/2ox}$ = 1.32 V; $E_{1/2re}$ = −0.35 V.

**(5,10,15-Tris(2.6-dichlorophenyl)corrolato)(oxo)molybdenum(V) (1b).** A solution of $H_3$(tdcc) (50 mg, 0.07 mmol) in Decalin (50 mL) was heated to 170−180 °C, followed by the addition of $Mo(CO)_6$ (0.073gr, 0.3 mmol). TLC examinations (silica gel, *n*-hexane/$CH_2Cl_2$ = 2:1) revealed that the starting material was fully consumed within 1 h of reaction. Solvent evaporation and crystallization from a benzene/*n*-hexane mixture yielded 38.4 mg (65%) of dark red crystals of (tdcc)Mo(O), **1b**.

UV−vis ($CH_2Cl_2$, $\lambda_{max}$ ($\epsilon \times 10^{-4}$): 436 (5.38), 512 (0.29), 550 (0.82), 582 nm (1.38). MS (DCI$^-$): *m/z* cluster of isotopes, centered at 843 ([M$^-$], 100%). EPR: $g$ = 1.972, $A^{14}{}_{N}$ = 0.266 mT, $A^{97}{}_{Mo}$ = 4.68 mT. Electrochemistry: $E_{1/2ox}$ = 1.04, 1.4 V; $E_{1/2re}$ = −0.49 V.

**Antimony Corroles. (5,10,15-Trispentafluorophenylcorrolato)(*trans*-bispyridine)antimony(III) (2a).** An about 3-fold excess of $SbCl_3$ (86 mg, 0.38 mmol) was added to a pyridine solution (5 mL) of **1** (100 mg, 0.126 mmol) in one portion. TLC examinations (silica gel, *n*-hexane/$CH_2Cl_2$=2:1) revealed that the starting material was fully consumed within 10 min at 100 °C. Solvent evaporation and crystallization from $CH_2Cl_2$/pyridine/*n*-heptane mixtures yielded 109 mg (95%) of (tpfc)Sb(pyr), **2a**.

UV−vis (pyridine) $\lambda_{max}$ ($\epsilon \times 10^{-4}$): 405 (3.43), 425 (14.78), 606 nm (1.22). MS−Maldi (TOF LD$^-$) (*m/z*): 914 ([M$^-$ − 2 pyridine], 100%). $^1$H NMR (pyridine-$d_5$, 300 MHz): $\delta$ 9.39 (overlapping doublets, 4H), 9.13 (d, $J$ = 4.5 Hz, 2H), 9.03 (d, $J$ = 3.9 Hz, 2H). $^1$H NMR ($C_6D_6$, 300 MHz): $\delta$ 8.94 (d, $J$ = 4.2 Hz, 2H), 8.79 (d, $J$ = 4.8 Hz, 2H), 8.54 (d, $J$ = 4.8 Hz, 2H), 8.47 (d, $J$ = 4.2 Hz, 2H). $^{19}$F NMR (pyridine-$d_5$, 282 MHz): $\delta$ −138.35 (dd, $^3J$ = 24.7 Hz, $^4J$ = 7.1 Hz, 2F, *o*-F), −138.67 (unresolved dd, 2F, *o*-F), −138.85 (dd, $^3J$ = 24.7 Hz, $^4J$ = 7.1 Hz, 2F, *o*-F), −154.05 (dt, $J$ = 21.4 Hz, 2F, *p*-F), −154.33 (t, $J$ = 21.2 Hz, 1F, *p*-F), −162.77 (dt, $J$ = 22.6 Hz, 6F, *m*-F). $^{19}$F NMR ($C_6D_6$, 282 MHz): $\delta$ −137.9 (dd, $^3J$ = 24.7 Hz, $^4J$ = 7.1 Hz, 3F, *o*-F), −138.32 (dd, $^3J$ = 24.7 Hz, $^4J$ = 7.1 Hz, 1F, *o*-F), −138.47 (dd, $^3J$ = 24.7 Hz, $^4J$ = 7.1 Hz, 2F, *o*-F), −152.67 (dt, $J$ = 21.2 Hz, 3F, *p*-F), −161.93 (dt, $^3J$ = 22.6 Hz, $^4J$ = 7.3 Hz, 4F, *m*-F), −162.37 (t, $^3J$ = 22.6 Hz, $^4J$ = 7.1 Hz, 2F, *m*-F).

**(5,10,15-Trispentafluorophenylcorrolato)(oxo)antimony(V) (2b).** A 3-fold excess of PhI(OAc)$_2$ (10.6 mg, 0.033 mmol) was added in one portion to a well-stirred solution of **2a** (10 mg, 0.011 mmol) in $CH_2Cl_2$. The color changed from green to red within 10 min. The solvent was evaporated, and the product was purified by column chromatography on silica gel with a mixture of *n*-hexane/$CH_2Cl_2$ (5:1) as eluent. Crystallyzation from a $CH_2Cl_2$/*n*-heptane mixture yielded 8 mg (75%) of (tpfc)Sb(O) as a red powder. Alternatively, **2b** was obtained in quantitative yields from solutions of **2a** that were left to stir under aerobic conditions for a few days.

UV−vis (THF) $\lambda_{max}$ ($\epsilon \times 10^{-4}$): 406 (9.73), 568 (1.42), 590 nm (1.43). MS−Maldi (TOF LD$^-$): *m/z* 930 ([M$^-$], 100%). $^1$H NMR ($C_6D_6$, 300 MHz): $\delta$ 8.54 (d, $J$ = 4.3 Hz, 2H), 8.45 (d, $J$ = 4.0 Hz, 2H), 8.14 (d, $J$ = 4.3 Hz, 2H), 8.08 (d, $J$ = 4.0 Hz, 2H). $^{19}$F NMR ($C_6D_6$, 282 MHz): $\delta$ −136.55 (d, $J$ = 25.4 Hz, 1F, *o*-F), −137.69 (d, $J$ = 23.1 Hz, 2F, *o*-F), −138.12 (d, $J$ = 19.2 Hz, 1F, *o*-F), −138.61(d, $J$ = 24.3 Hz, 2F, *o*-F), −151.61 (t, $J$ = 21.4 Hz, 2F, *p*-F), −152.93 (t, $J$ = 21.4 Hz, 1F, *p*-F), −161.34 (dt, $J$ = 19.2 Hz, 2F, *m*-F), −161.67 (t, $J$ = 23.1 Hz, 1F, *m*-F), −164.46 (dt, $J$ = 19.7 Hz, 2F, *m*-F), −164.77 (t, $J$ = 20.3 Hz, 1F, *m*-F).

**(5,10,15-Trispentafluorophenylcorrolato)(*trans*-difluoro)antimony(V) (2c).** A solution of **2a** (10 mg, 0.011 mmol) in $CH_2Cl_2$ (15 mL) was treated with aqueous HF (48%, 15 mL) The mixture was stirred for 24 h at room temperature, during which the color changed from green to violet, and TLC examinations (silica gel, *n*-hexane/$CH_2Cl_2$ = 2:1) revealed quantitative disappearance of the starting material. Crystallization from $CH_2Cl_2$/*n*-heptane mixtures yielded 10 mg (97%) of (tpfc)Sb(F)$_2$. Dark violet X-ray quality crystals of **2c** were obtained from a mixture of THF and *n*-heptane.

(25) Stavitski, E.; Berg, A.; Mahammed, A.; Gross, Z.; Levanon H. Manuscript in preparation.

UV−vis (THF) $\lambda_{max}$ ($\epsilon \times 10^{-4}$): 392 (9.32), 412 (32.05), 566 (3.14), 588 nm (3.73). MS−Maldi (TOF LD$^-$): $m/z$ 952 ([M$^-$], 100%). $^1$H NMR ($CDCl_3$, 300 MHz): $\delta$ 9.64 (d, $J$ = 4.3 Hz, 2H), 9.21(d, $J$ = 4.8 Hz, 2H), 9.14 (d, $J$ = 4.3 Hz, 2H), 9.03 d, $J$ = 4.8 Hz, 2H). $^{19}$F NMR ($CDCl_3$, 282 MHz): $\delta$ −105.43 (s, 2F, from Sb−F), −136.12 (unresolved dd, 2F, *o*-F), −136.27 (dd, $^3J$ = 21.2 Hz, $^4J$ = 6.2 Hz, 4F, *o*-F), −150.78 (t, $J$ = 20.9 Hz, 2F, *p*-F), −150.89 (t, $J$ = 20.9 Hz, 1F, *p*-F), −160.87 (dt, $^3J$ = 21.2 Hz, $^4J$ = 7.05 Hz, 6F, *m*-F).

**X-ray Diffraction.** The X-ray diffraction measurements were carried out on a Nonius KappaCCD diffractometer using graphite-monochromated Mo K$\alpha$ radiation ($\lambda$ = 0.7107 Å). The crystalline samples of the analyzed compounds were covered with a thin layer of light oil and freeze-cooled to ca. 110 K to minimize possible solvent escape, structural disorder, and thermal motion effects and to increase the precision of the results. The crystal structures were solved by direct and Patterson methods and refined by full-matrix least squares. All non-hydrogen atoms were refined anisotropically, and the hydrogens were located in idealized positions. Compounds **1a** and **2c** crystallized as di-benzene and THF solvates, respectively.

**Crystal Data. 1a**: $C_{37}H_8F_{15}N_4MoO{\cdot}2C_6H_6$, $M$ = 1061.63, triclinic, space group $P\bar{1}$, $a$ = 8.4738(1) Å, $b$ = 13.6757(3) Å, $c$ = 19.5250(5) Å, $\alpha$ = 70.772(1)°, $\beta$ = 84.544(2)°, $\gamma$ = 72.697(1)°, $V$ = 2039.74(7) Å$^3$, $Z$ = 2, $T$ = 110(2) K, $D_c$ = 1.728 g cm$^{-3}$, $\mu$(Mo K$\alpha$) = 0.44 mm$^{-1}$, 9397 unique reflections to $2\theta_{max}$ = 56.4°, 631 refined parameters, $R_1$ = 0.041 for 7629 observations with $I > 2\sigma(I)$, $R_1$ = 0.057 ($R_2$ = 0.105) for all unique data, $|\Delta\rho|_{max}$ = 0.86 e/Å$^3$.

**2c**: $C_{37}H_8F_{17}N_4Sb{\cdot}C_4H_8O$, $M$ = 1025.33, monoclinic, space group $P2_1/c$, $a$ = 18.1025(1) Å, $b$ = 15.6779(2) Å, $c$ = 13.9353(2) Å, $\beta$ = 112.1721(5)°, $V$ = 3662.52(7) Å$^3$, $Z$ = 4, $T$ = 110(2) K, $D_c$ = 1.859 g cm$^{-3}$, $\mu$(Mo K$\alpha$) = 0.88 mm$^{-1}$, 8700 unique reflections to $2\theta_{max}$ = 55.7°, 577 refined parameters, $R_1$ = 0.035 for 7504 observations with $I > 2\sigma(I)$, $R_1$ = 0.043 ($R_2$ = 0.095) for all unique data, $|\Delta\rho|_{max}$ = 1.24 e/Å$^3$. The THF solvent is partly disordered.

**Table 3.** Bond Distances (Å) and Bond Angles (deg) in the Metal Coordination Sphere of the Crystalline Complexes **1a** and **2c**

| | | | |
|---|---|---|---|
| **1a**[a] | | | |
| Mo−O | 1.684(2) | Mo−N21 | 2.035(2) |
| Mo−N22 | 2.038(2) | Mo−N23 | 2.039(2) |
| Mo−N24 | 2.033(2) | | |
| O−Mo−N21 | 111.5(1) | O−Mo−N22 | 110.8(1) |
| O−Mo−N23 | 110.2(1) | O−Mo−N24 | 111.6(1) |
| N21−Mo−N22 | 83.2(1) | N21−Mo−N23 | 137.7(1) |
| N21−Mo−N24 | 74.9(1) | N22−Mo−N23 | 89.0(1) |
| N22−Mo−N24 | 136.9(1) | N23−Mo−N24 | 83.3(1) |
| **2c**[b] | | | |
| Sb−F1 | 1.940(1) | Sb−F2 | 1.932(1) |
| Sb−N21 | 1.979(2) | Sb−N22 | 1.971(1) |
| Sb−N23 | 1.974(2) | Sb−N24 | 1.979(1) |
| F1−Sb−F2 | 177.3(1) | | |
| F1− Sb−N21 | 90.7(1) | F1−Sb−N22 | 90.3(1) |
| F1−Sb−N23 | 88.0(1) | F1−Sb−N24 | 89.6(1) |
| F2−Sb−N21 | 92.0(1) | F2−Sb−N22 | 89.4(1) |
| F2−Sb−N23 | 89.4(1) | F2−Sb−N24 | 91.1(1) |
| N21−Sb−N22 | 91.6(1) | N21−Sb−N23 | 171.4(1) |
| N21−Sb−N24 | 79.7(1) | N22−Sb−N23 | 96.9(1) |
| N22−Sb−N24 | 171.3(1) | N23−Sb−N24 | 91.8(1) |

[a] The pentacoordinated metallo-corrole core has a domed conformation. [b] The hexa-coordinated metallo-corrole core has a nearly planar conformation.

Table 3 summarizes the main observed bond distances and angles for the two metallo-corrole complexes (all covalent parameters are detailed in the Supporting Information). They reflect the domed conformation in **1a** and nearly planar conformation in **2c**.

**Acknowledgment.** This research was supported by the Israel Science Foundation, Grant Nos. 330/04 (Z.G.) and 68/01 (I.G.).

**Supporting Information Available:** Crystallographic data in CIF format. This material is available free of charge via the Internet at http://pubs.acs.org.

IC051483G